Ionics (2019) 25:3473–3491
https://doi.org/10.1007/s11581-018-2817-7

ORIGINAL PAPER

Synthesis and investigation of quinazoline derivatives based on 8-hydroxyquinoline as corrosion inhibitors for mild steel in acidic environment: experimental and theoretical studies

M. Rbaa[1] · M. Galai[2] · F. Benhiba[3] · I. B. Obot[4] · H. Oudda[3] · M. Ebn Touhami[2] · B. Lakhrissi[1] · A. Zarrouk[5]

Received: 30 August 2018 / Revised: 2 November 2018 / Accepted: 25 November 2018 / Published online: 12 December 2018

Abstract

HCl pickling treatment is utilized to remove mill scales from mild steel (MS) surface at different temperatures up to 328 ± 2 K. In order to minimize the metal dissolution, newly multifunctional heterocycles based on 8-hydroxyquinoline namely *3-((8-hydroxyquinolin-5yl)-methyl)-2-phenylquinazolin-4(3H)-one (HQ-ZH)*, *3-((8-hydroxyquinliene-5-yl)-2-(4-nitrophenyl)-quinazolin-4(3H)-one (HQ-ZNO$_2$)*, and *2-(2-hydroxyphenyl)-3-((8-hydroxyquinolin-5-yl)-methyl)-quinazolin-4(3H)-one (HQ-ZOH)* have been synthesized and characterized by Fourier transform infrared (FT-IR), ^{1}H, ^{13}C *NMR*, and elemental analysis. Their anticorrosive performance for the mild steel in 1 M HCl medium has been determined by electrochemical and theoretical investigations. *HQ-ZH*, *HQ-ZOH*, and *HQ-ZNO$_2$* act as excellent inhibitors for MS in 1 M HCl. In addition, the surface of the mild steel has been analyzed by the UV-visible and SEM. The experimental results were correlated with theoretical studies.

Keywords Synthesis · Quinazolinone derivatives · Corrosion inhibition · Electrochemical techniques · Theoretical studies · SEM

Introduction

Mild steel is widely used for the manufacture of a wide variety of metal structures and equipment. It is economical and easily available on the market [1]. In industries, during various industrial processes such as pickling, cleaning, etching, and acidification of oil wells, the mild steel is subjected to corrosion [2]. However, in recent years, it is preferable to use heterocyclic compounds as corrosion inhibitors to overcome this corrosion problem [3, 4]. In aggressive media (HCl, H_2SO_4, ...), the compounds that reduce the degradation of metallic materials can be distinguished into three types: surfactant inhibitors, organic inhibitors and inorganic inhibitors [5–16]. Among the commonly available acids are hydrochloric acid, which is replaced by sulfuric acid [17] and other acids such as nitric acid, perchloric acid, citric acid acetic acid, and formic acid, which are used only for specific applications.

The choice of effective mild steel corrosion inhibitors was based on their mechanism of action and their ability to produce electrons [18]. Moreover, the heterocyclic organic inhibitors have many advantages for the inhibition of corrosion in an acid medium [19]. Quinazolinone derivatives are the effectiveness of corrosion inhibition on the mild steel surface in acidic media. Many researchers have investigated the quinazoline compounds as corrosion inhibitors, since their nitrogen atoms with a free pair of electrons act as potential sites for bonding with metals, thereby inhibiting corrosion [20–27].

The novelty of this work lies in the synthesis of three new quinazolinone compounds derivatives of 8-hydroxyquinoline to obtain a new variety of multifunctional heterocycles, having several reactive sites for use as corrosion inhibitors of mild

✉ A. Zarrouk
azarrouk@gmail.com

[1] Laboratory Agro-Resources, Polymers and Process Engineering, Department of Chemistry, Faculty of Sciences, Ibn Tofail University, PO Box 133, 14000 Kénitra, Morocco

[2] Laboratory of Materials Engineering and Environment: Application and Modeling, Faculty of Sciences, Ibn Tofail University, PO Box 133, 14000 Kénitra, Morocco

[3] Laboratory of separation processes, Faculty of science, University Ibn Tofail, PO Box 133, 14000 Kénitra, Morocco

[4] Centre of Research Excellence in Corrosion, King Fahd University of Petroleum and Minerals, Dhahran, Saudi Arabia

[5] Laboratory of Materials, Nanotechnology and Environment, Faculty of Sciences, Mohammed V University, Av. Ibn Battuta. B.P 1014, Rabat, Morocco

steel in acidic medium. The corrosion inhibiting action find out about of these compounds was evaluated by electrochemical methods (potentiodynamic polarization, impedance spectroscopy) and gravimetric methods (mass loss). in addition, *MC* simulations and *DFT* calculations are employed to discuss the adsorption configuration to give an explanation for the corrosion inhibition mechanism of utilized inhibitors on the MS surface.

Procedure

General information

Unless otherwise stated, all the reagents and solvents used in this study were obtained from Sigma-Aldrich Chemical Company (Spain or France). Melting points were determined on Banc Kofler apparatus and are uncorrected. The recording of NMR spectra was performed on a Bruker Advanced 300 WB at 300 MHz for solutions in Me_2SO-d_6 and chemical shifts are given in δ_{ppm} with reference to tetramethylsilane (TMS) as an internal standard. The elemental composition (carbon, hydrogen, and nitrogen) was determined on a Perkin-Elmer Model 240 CHN Analyzer. The progress of the reaction is followed by chromatography with thin layer (TLC) of silica 60 F254 (E. Merck).

The mild steel samples were used with C, 0.11; Si, 0.24; Mn, 0.47; Cr, 0.12; Mo, 0.02; Ni, 0.1; Al, 0.03; Cu, 0.14; Co, < 0.012; V, < 0.003; W, 0.06; Fe, balance; and the remainder of iron. Before any measurement, they were abraded with a series of emery paper grades 180–1200. The specimens are thoroughly washed with double distilled water, degreased with acetone and then dried. The aggressive solution 1 M HCl was prepared by the dilution of concentrated HCl (37%) analytical grade with bi-distilled water.

Synthesis methods

A mixture of quinazolinone derivatives (1 eq) and 5-chloromethyl-8-hydroxy-quinolinehydrochloride (2 eq) in 50 mL of pure tetrahydrofuran in the presence of triethylamine (2 eq) was refluxed for 24 h under stirring. The reaction was monitored by CCM. After evaporation of the solvent, the residue obtained was hydrolyzed with a saturated NaCl solution (20 mL), extracted with chloroform (3 × 20 mL). The combined organic layers were dried over anhydrous magnesium sulfate, filtered, and evaporated in vacuum to give crudes products as solids. The purification of the product was realized by chromatography on a silica gel column utilizing dichloromethane/hexane (85:15, *v*/*v*), and then recrystallized from absolute ethanol, (Scheme 1).

Corrosion tests

The electrochemical techniques have been described in the same previous public work [15]. The values of performance $\eta_{PDP}(\%)$ are calculated utilizing Eq. 1:

$$\eta_{PDP}(\%) = \left(\frac{i_{corr} - i'_{corr}}{i_{corr}}\right) \times 100 \quad (1)$$

where i_{corr} is the corrosion current density in the absence of *HQ-ZH*, *HQ-ZNO*$_2$, and *HQ-ZOH*, and i'_{corr} is the corrosion current density with *HQ-ZH*, *HQ-ZNO*$_2$ and *HQ-ZOH* [15].

The conventional electrochemical impedance spectroscopy (*SIE*) was run at a frequency ranging from 100 kHz up to 100 mHz with a.c. amplitude 10 mV at OCP [15]. All the electrochemical experiments were performed at room temperature (298 ± 2 K) but potentiodynamic polarization study was carried out at various temperature range from 298 to 328 ± 2 K for calculating kinetic and thermodynamic parameters. Nyquist plots were made from these experiments. The best fit of the experiments was done utilizing Bouckamp program. The Eq. 2 was utilized to estimate the $\eta_{EIS}\eta_{EIS}$ *(%)*:

$$\eta_{EIS}(\%) = \left(\frac{R_p - R'_p}{R_p}\right) \times 100 \quad (2)$$

where R_pR_p is of polarization resistance in the presence of *HQ-ZH*, *HQ-ZNO*$_2$, and *HQ-ZOH*, and R'_p is the value of polarization without inhibitors.

Surface analysis

Scanning electron microscopy

After immersing in a solution of HCl (1 M) for 6 h except and with optimum concentration (1 mM) of quinazoline derivatives, the surface of the steel was analyzed by way of scanning electron microscopy (*SEM*). The method of sample preparation in our steel was identical to that described in the "General information" section. The SEM images were performed on the surface of the MS panels in the absence and in the presence of *HQ-ZH*, *HQ-ZNO*$_2$, and *HQ-ZOH* to analyze the morphology of the deposited protective layers.

UV-visible spectra

To discover more data on the bonding mechanism of MS surfaces/compounds/aggressive environment, corrosion protection was also investigated by means of ultraviolet-visible spectrophotometry (*UV-Vis*), before and after immersion of

Scheme 1 Synthetic route for the preparation of quinazoline derivatives based on 8-hydroxyquinoline

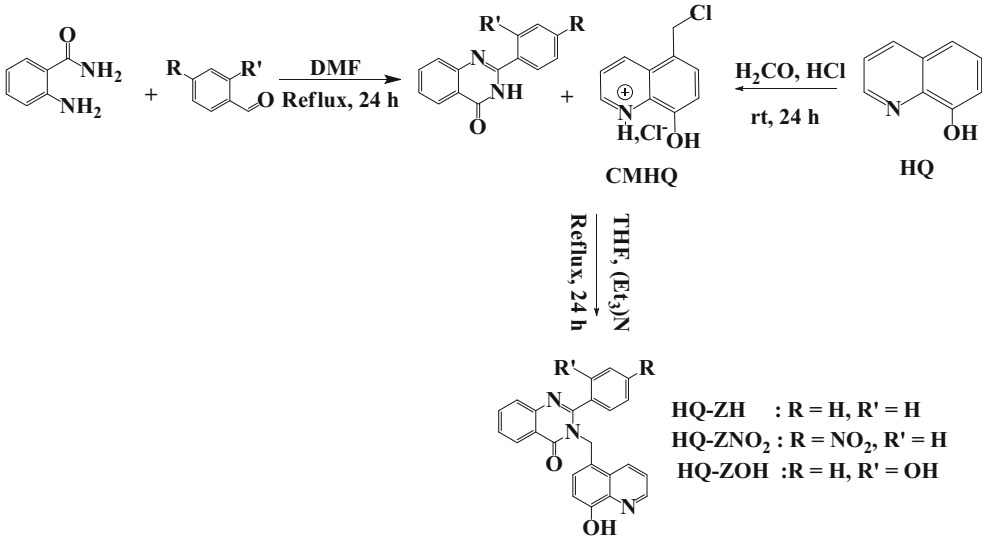

the MS sample for 24 h. The Jenway ultraviolet-visible spectrophotometer (series 67) was once utilized for this analysis.

Theoretical studies

Density functional theory

The GAUSSIAN 09 W [11] software was utilized to process quantum parameters, the geometry of the studied molecules was fully optimized by the DFT method at *B3LYP* level with the bases *6-31G (d, p)* and *6-311G (d, p)* in two gaseous and aqueous phases.

The values of the energies of the *HOMO* and *LUMO* orbitals were determined by the electronic affinity and ionization energy [28]:

$$IP = -E_{HOMO} \tag{3}$$

$$EA = -E_{LUMO} \tag{4}$$

In order to find the values of the electronegativity and the overall hardness of the inhibitory molecule, the values of A and I are treated by the eq. (5, 6), [29, 30]:

$$\chi = \frac{IP + EA}{2} \tag{5}$$

$$\eta = \frac{IP - EA}{2} \tag{6}$$

The number of transferring electrons (ΔN) was calculated according to eq. 7.

$$\Delta N = \frac{\phi - \chi_{\text{inh}}}{2(\eta_{Fe} + \eta_{\text{inh}})} \tag{7}$$

ϕ is the work function utilized as the measure of electronegativity of iron, and $\eta_{Fe} = 0$. The value of $\phi = 4.82$ eV for *Fe (110)* surface which is reported to have higher stabilization energy [31].

The local reactivity of molecular (electrophilic and nucleophilic attacks) were obtained by Fukui functions using the following equations [32]:

$$f_i\left(\overrightarrow{r}\right)^{+} = q_i(N+1) - q_i(N) \tag{8}$$

$$f_i\left(\overrightarrow{r}\right)^{-} = q_i(N) - q_i(N-1) \tag{9}$$

where q_i *(N+ 1)*, q_i *(N)*, q_i *(N-1)* are charge values of atom *i* for cation, neutral and anion, respectively. Fukui indices were performed by the method *DFT/B3LYP / 6-31G (d, p)* [33].

Monte Carlo simulations

Metropolis Monte Carlo simulations utilizing simulated annealing procedure were carried out to quantify the adsorption of *HQ-ZH*, *HQ-ZNO*$_2$, and *HQ-ZOH* on *Fe (110)* surface. The simulation box consisted of 5 layers of iron atoms cleaved along the (110) plane. A supercell of (10 × 10) was created and vacuum layer of 50 nm height was fabricated. Optimized *HQ-ZH*, *HQ-ZNO*$_2$, and *HQ-ZOH* molecules were positioned near the surface of *Fe (110)* plane utilizing the simulated annealing adsorption locator module with COMPASS force field. The simulations were performed under fine convergence conditions, while each simulation went through 5 cycles at 50,000 steps per cycle. Lowest adsorption energies were obtained and documented for *HQ-ZH*, *HQ-ZNO*$_2$, and *HQ-ZOH* as they interact with the Fe surface.

Results and discussions

Chemistry

Data, value and validation

Characterization of 3-((8-hydroxyquinolin-5-yl)-methyl)-2-phenylquinazolin-4(3H)-one (HQ-ZH) Yield: 80%, Aspect: white solid, Mp = 162–164 °C, R_f = 0.25 (hexane/ethanol, 70/30: *v*/*v*). IR (ν_{max}/cm^{-1}): 1300–1600 (C=C), 1419.41 (C=N), 3248.08 (OH bonded), 2367.24–2888.57 (C-H), 1624.09 (CH_2). ^{1}H (300 MHz, DSMO-d_6): δ_{ppm} = 5.12 (S, 2 H, CH_2), 5.61 (S, 1 H, OH), 7.59-7.61-7.63-8.81-8.82 (m, 5 H, ArH-quinoline) 7.25-7.60-7.91-8.99-9.02 (m, 9 H, ArH-quinazolinone). ^{13}C (300 MHz, DSMO-d_6): δ_{ppm} = 69.53 (CH_2), 148.76 (ArC-OH), 152.35 ((N=C(Ph)N), 153.91 (C=O), 126.90–126.99-127,74-128.28-13.52-132.69-133.31 (ArCH-quinazolinone), 119.69-129.26-148.28 (ArC-quinazolinone), 112.55-122.156-13.71-148.40 (ArCH-quinoline), 127.74-122.74-139.31 (ArC-quinoline).

Analysis elemental:

- Calculated: C, 75.97%; H, 4.52%; N, 11.08%.
- Obtained: C, 76.01%, H, 4.53%, N, 11.12%.

Characterization of 3-((8-hydroxyquinolin-5-yl)-2-(4-nitrophenyl)-quinazolin-4(3H)-one (HQ-ZNO$_2$) Yield: 65%, Aspect: yellow solid, Mp = 169–171 °C, R_f = 0.29 (hexane/ethanol, 70/30: *v*/*v*).

IR(ν_{max}/cm^{-1}): 1518.39–1642.49 (C=C), 1451.13 (C=N), 3414.35 (OH bonded), 2036.30 (C-H), 1624.49 (CH_2). ^{1}H (300 MHz, DSMO-d_6): δ_{ppm} = 5.22 (S, 2 H, CH_2), 5.72 (S, 1 H, OH), 7.12-7.24-7.62-8.92-9.98 (m, 5 H, ArH- quinoline), 7.63-7.65-8.86-8.88-8.89 (m, 8 H, ArH-quinazolinone). ^{13}C (300 MHz, DSMO-d_6): δ_{ppm} = 46.12 (CH_2), 152.87 (ArC-OH), 152.19 (C=O) 151.00 ((N=C(ph)N), 124.64-125.97-126.92-127.39-128.64-138.76 (ArCH-quinazolinone), 121.78-133.93-145.88-148.0 (ArCquinazolinone), 111.24-122.03-127.18-

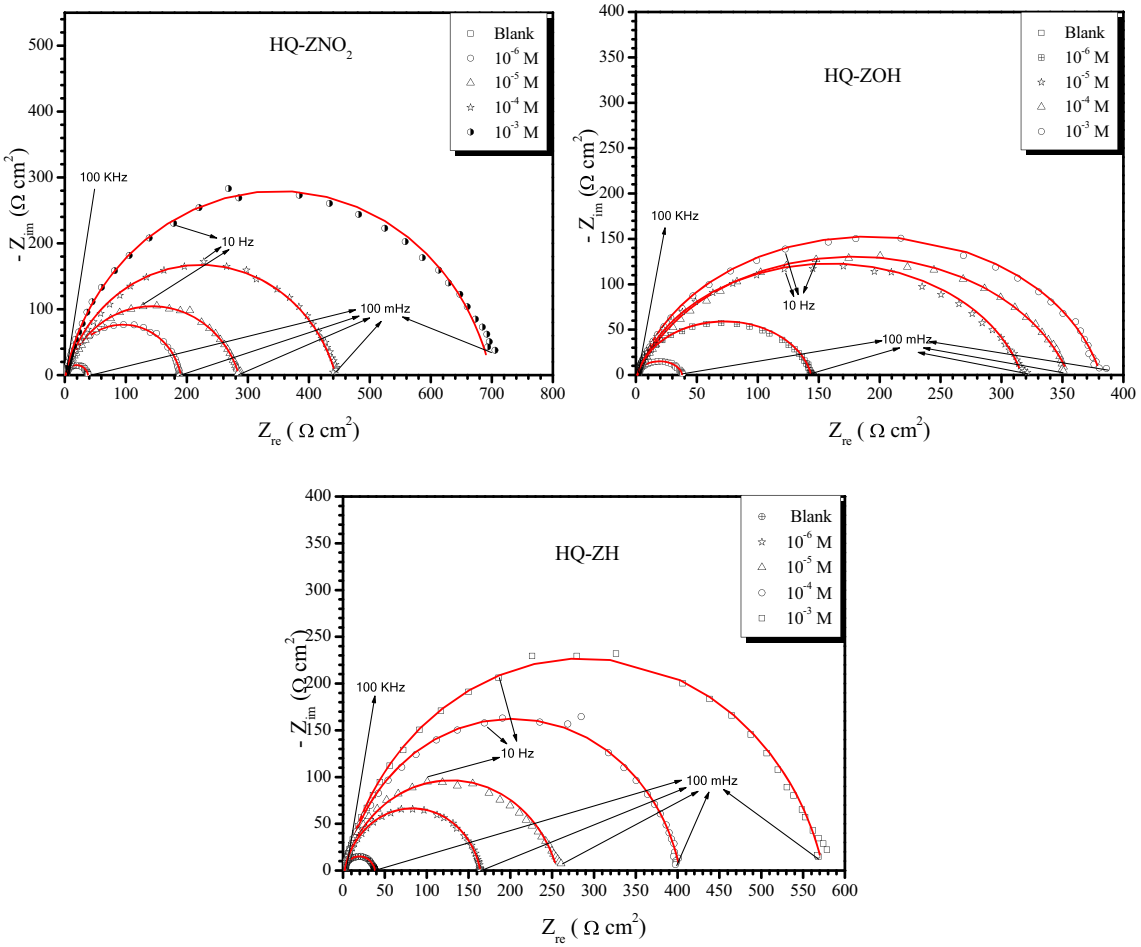

Fig. 1 Nyquist plots for MS in 1 M HCl with 0–10^{-3} M concentrations of *HQ-ZH*, *HQ-ZNO$_2$*, and *HQ-ZOH* at *OCP* and 298 ± 2 K

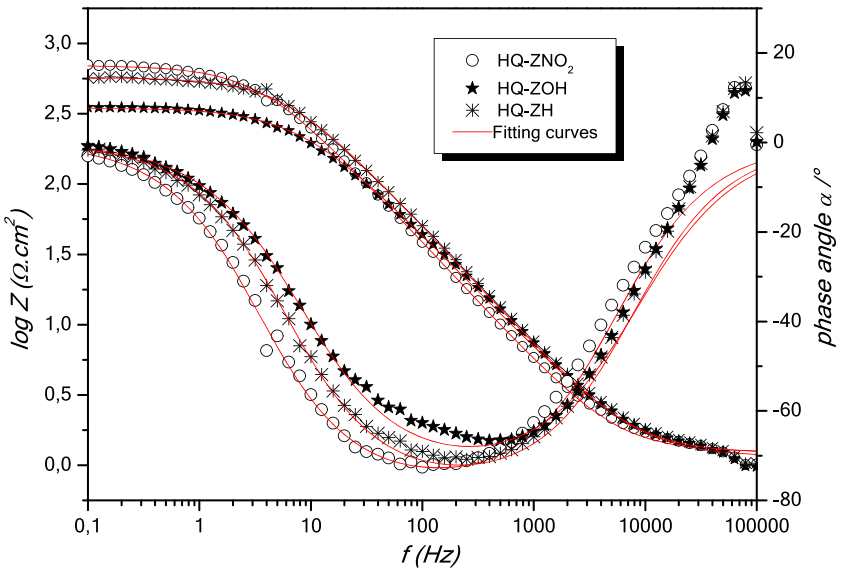

Fig. 2 Equivalent circuit for MS/molar HCl/substituted quinazoline compounds

130.30-152.188 (ArCH-quinoline), 127.18-127.78-128.77 (ArC-quinoline).

Analysis elemental:

- Calculated: C, 67.92%; H, 3.80%; N, 13.20%.
- Obtained: C, 67.95%, H, 3.79%, N, 13.15%.

Characterization of 2-(2-hydroxyphenyl)-3-((8-hydroxyquinolin-5-yl)-methyl)-quina-zolin-4 (3H)-one (HQ-ZOH) Yield: 70%, Aspect: brown solid, Mp = 149–151 °C, $R_{f\ =}$ 0.31 (hexane/ethanol, 70/30: *v*/*v*). IR: 1723.95–1777.87 (C=C), 1505.86 (C=N), 3641.79 (OH bonded), 2037.54 (C-H), 1794.99 (CH_2). ^{1}H (300 MHz, DSMO-d_6): $\delta_{ppm} = 5.33$ (S, 2 H, CH_2), 6.43 (S, 2 H, OH), 7.08-7.41-7.64-8.66-8.89 (m, 5 H, ArH-quinoline), 7.06-7.38-7.63-7.66-7.67-8.65-8.68 (m, 8 H, ArH-quinazolinone).

^{13}C (300 MHz, DSMO-d_6): $\delta_{ppm} = 61.10$ (CH_2), 152.04 (ArC-OH quinoline), 147.99 (ArC-OH benzene rang of quinazolinone) 155.74 (C=O) 153.06 ((N=C(ph)N), 122.44-126.11-127.60-128.491-128.84-130.46-134.59 (ArCH-quinazolinone), 111.62-123.11-140.90 (ArC-quinazolinone), 116.11-126.11-128.62-134.59-139.26 (ArCH-quinoline), 127.72-130.02-138.08 (ArC-quinoline).

Analysis elemental:

- Calculated: C, 72.90%; H, 4.33%; N, 10.63%.
- Obtained: C, 72.88%, H, 4.35%, N, 10.53%.

Table 1 Parameters of impedance and the corrosion inhibition performance of MS in 1 M HCl at different concentrations of *HQ-ZH*, *HQ-ZNO*$_2$, and *HQ-ZOH*

Medium	*[C]* (M)	R_s (Ω cm^2)	R_p (Ω cm^2)	C_{dl} (μF cm^{-2})	*n*	η_{EIS} (%)
Blank	1	2.08	35.0	298.0	0.78	–
HQ-ZNO$_2$	10^{-3}	1.23	697.6	65.73	0.86	95.0
	10^{-4}	1.30	442.7	42.01	0.82	92.0
	10^{-5}	1.02	284.5	64.26	0.80	87.7
	10^{-6}	1.07	189.1	86.11	0.86	81.5
HQ-ZOH	10^{-3}	1.46	379.8	70.03	0.86	90.8
	10^{-4}	1.74	353.4	58.45	0.80	90.1
	10^{-5}	1.35	315.4	72.14	0.84	88.9
	10^{-6}	1.22	142.6	116.0	0.88	75.4
HQ-ZH	10^{-3}	1.59	573.0	47.43	0.85	93.9
	10^{-4}	1.95	401.0	50.80	0.86	91.3
	10^{-5}	1.60	255.6	111.0	0.82	86.3
	10^{-6}	1.91	162.1	76.00	0.87	78.4

Electrochemical impedance spectroscopy measurements

EIS measurements were performed to study the impedance parameters MS in 1 M HCl at various concentrations of *HQ-ZH*, *HQ-ZNO*$_2$, and *HQ-ZOH* at 298 ± 2 K. Before each test, the working electrode was immersed in the test solution for 1/2 h at 298 ± 2 K to attain the steady potential. To analyze the impedance parameters from the experimental outcomes, the data were fitted to the electrical equivalent circuit. Figure 2 shows the used electrical equivalent circuit in the appearance and non-appearance of *HQ-ZH*, *HQ-ZNO*$_2$, and *HQ-ZOH*. The *EIS* curves (Nyquist) for MS with and without *HQ-ZH*, *HQ-ZNO*$_2$, and *HQ-ZOH* are shown in Fig. 1. According to

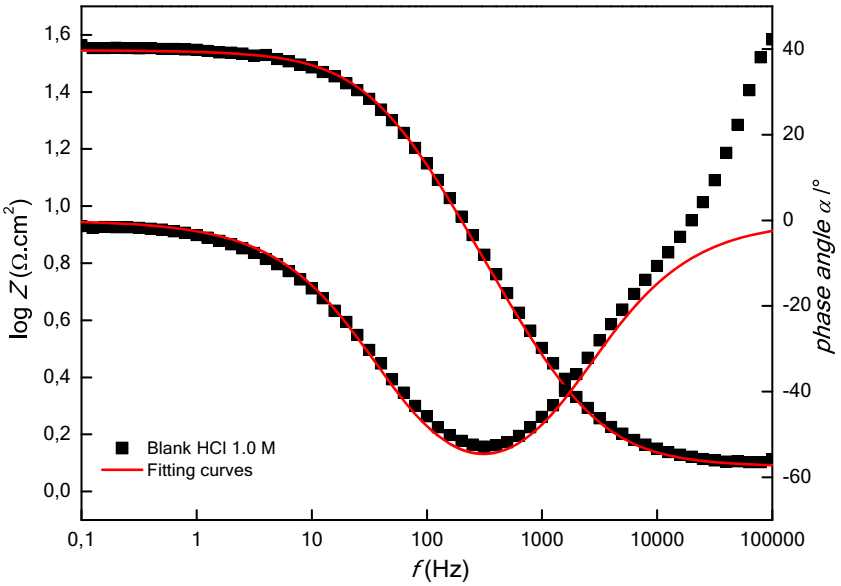

Fig. 3 Bode and phase diagrams of steel after immersion in HCl solutiondifferent concentrations of inhibitors and blank solution

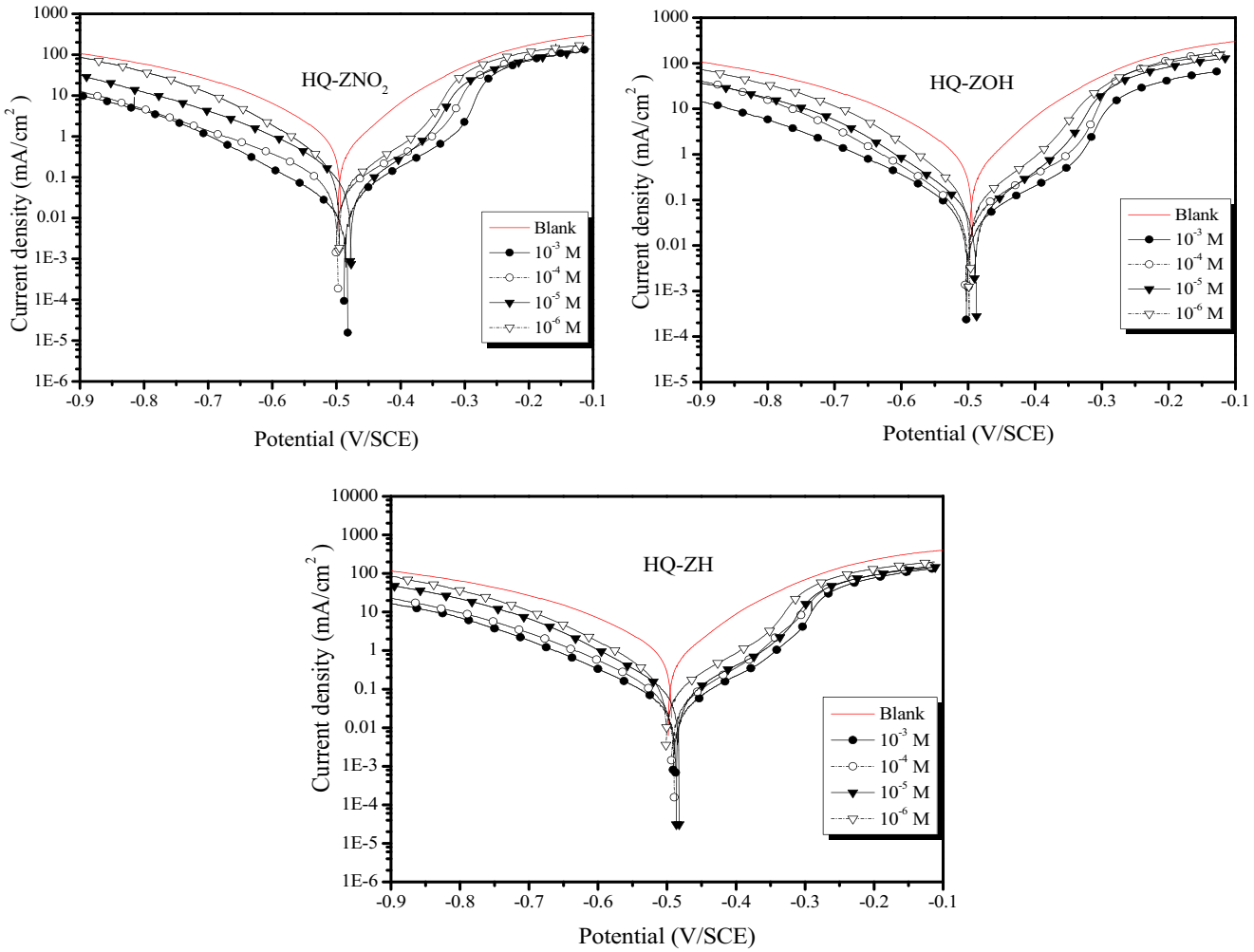

Fig. 4 Potentiodynamic polarization curves for MS in 1 M HCl containing different concentration of *HQ-ZH*, *HQ-ZNO*$_2$, and *HQ-ZOH* at 298 ± 2 K

Table 2 Polarization parameters for MS in 1 M HCl without and with different concentrations of *HQ-ZH*, *HQ-ZNO*$_2$, and *HQ-ZOH* at 298 ± 2 K

Medium	Conc (M)	-E_{corr} (mVSCE)	i_{corr} (μA cm^{-2})	-β_c (mV dec^{-1})	β_a (mV dec^{-1})	θ	η_{PDP} (%)
Blank	1	498	983	92	104	–	–
HQ-ZOH	10^{-3}	492	84	117	112	0.914	91.4
	10^{-4}	496	90	101	109	0.908	90.8
	10^{-5}	482	105	92	87	0.893	89.3
	10^{-6}	492	235	86	83	0.760	76.0
HQ-ZH	10^{-3}	482	55	110	94	0.944	94.4
	10^{-4}	485	77	101	87	0.922	92.2
	10^{-5}	477	128	95	82	0.869	86.9
	10^{-6}	492	160	93	78	0.837	83.7
HQ-ZNO$_2$	10^{-3}	480	40	98	85	0.959	95.9
	10^{-4}	495	70	106	98	0.928	92.8
	10^{-5}	471	120	110	85	0.878	87.8
	10^{-6}	490	180	114	75	0.817	81.7

these figures, all plots show only one time constant and the semicircular shape did not change after addition of *HQ-ZH*, *HQ-ZNO*$_2$, and *HQ-ZOH* [34]. This means that the corrosion reaction is under charge transfer control and the corrosion mechanism did not change. It can be seen from the Nyquist plots that the increase in inhibitor concentration resulted in the increase of diameter of Nyquist plots.

The equivalent circuit shown in Fig. 2 has been utilized to adapting of the experimental impedance data. The circuit includes constant phase elements (*CPE*), polarization resistance (R_p) and solution resistance (R_s). Generally, the double layer formed by the adsorption of inhibitors on the metal surface behaves like a *CPE* rather than a pure capacitor and, therefore, the capacitor has been replaced by *CPE* to fit more precisely the data of semicircle impedance. The admittance (Y_{CPE}) and the impedance (Z_{CPE}) of the *CPE* can be represented by the following relationships (10,11):

$$Y_{CPE} = Y_0(j\omega)^n \tag{10}$$

$$Z_{CPE} = \left(\frac{1}{Y_0}\right)\left[(j\omega)_n\right]^{-1} \tag{11}$$

Where Y_0 is the *CPE* constant, ω is the angular frequency; j is the imaginary number (i.e. $j^2 = -1$) and n is the phase shift (exponent) which is related to the degree of surface in homogeneity.

The derived impedance parameters are presented in Table 1.

In the light of the obtained results, we can make the following remarks:

The results in Table 1 show that the index values n in the presence of *HQ-ZH*, *HQ-ZNO*$_2$, and *HQ-ZOH* greater than that of white, which suggests that the inhomogeneity of the surface decreases in the presence of the organic inhibitors this can be explained by the formation of a film protector on the steel surface. In addition, R_p values increase progressively with inhibitor concentrations that are attributed due to the adsorption of inhibitors on the metal surface that isolate the metal from the electrolyte and protect against corrosion [35, 36].

Another important thing was observed that C_{dl} values decrease after adding *HQ-ZH*, *HQ-ZNO*$_2$, and *HQ-ZOH*. This also indicates that the thickness of the double layer increase with *HQ-ZH*, *HQ-ZNO*$_2$, and *HQ-ZOH* concentration, which is well explained by this formula [35]:

$$C_{dl} = \frac{\varepsilon_0 \varepsilon}{d} S \tag{12}$$

where, ε_0 is the permittivity of space, ε is the local dielectric constant, d is the film thickness and S is the surface area. From formula, it is found that C_{dl} is directly proportional to ε and inversely proportional to d. The C_{dl} value was decreased due to decrease in local dielectric constant because of replacement of water molecules (higher ε value) by the inhibitor molecules (lower ε value). The increase in thickness (d) of the electrical double layer was observed with increase in concentration of *HQ-ZH*, *HQ-ZNO*$_2$, and *HQ-ZOH* which also play an important role in decrease of C_{dl} value [36].

On the other hand, the corrosion inhibiting performance increases with the concentration of the inhibitors to reach an optimal value of 95%, 93.90%, and 90.8% respectively for *HQ-ZH*, *HQ-ZNO*$_2$, and *HQ-ZOH*. On the other hand, the *HQ-ZNO*$_2$ inhibitor has a good performance compared to *HQ-ZH* and *HQ-ZOH* respectively in 1 M of HCl medium. This was explained by the nature and position of the groups (-*NO*$_2$, -*OH*); para position gives a performance better than ortho position. The result was confirmed by the theoretical study (Fig. 3).

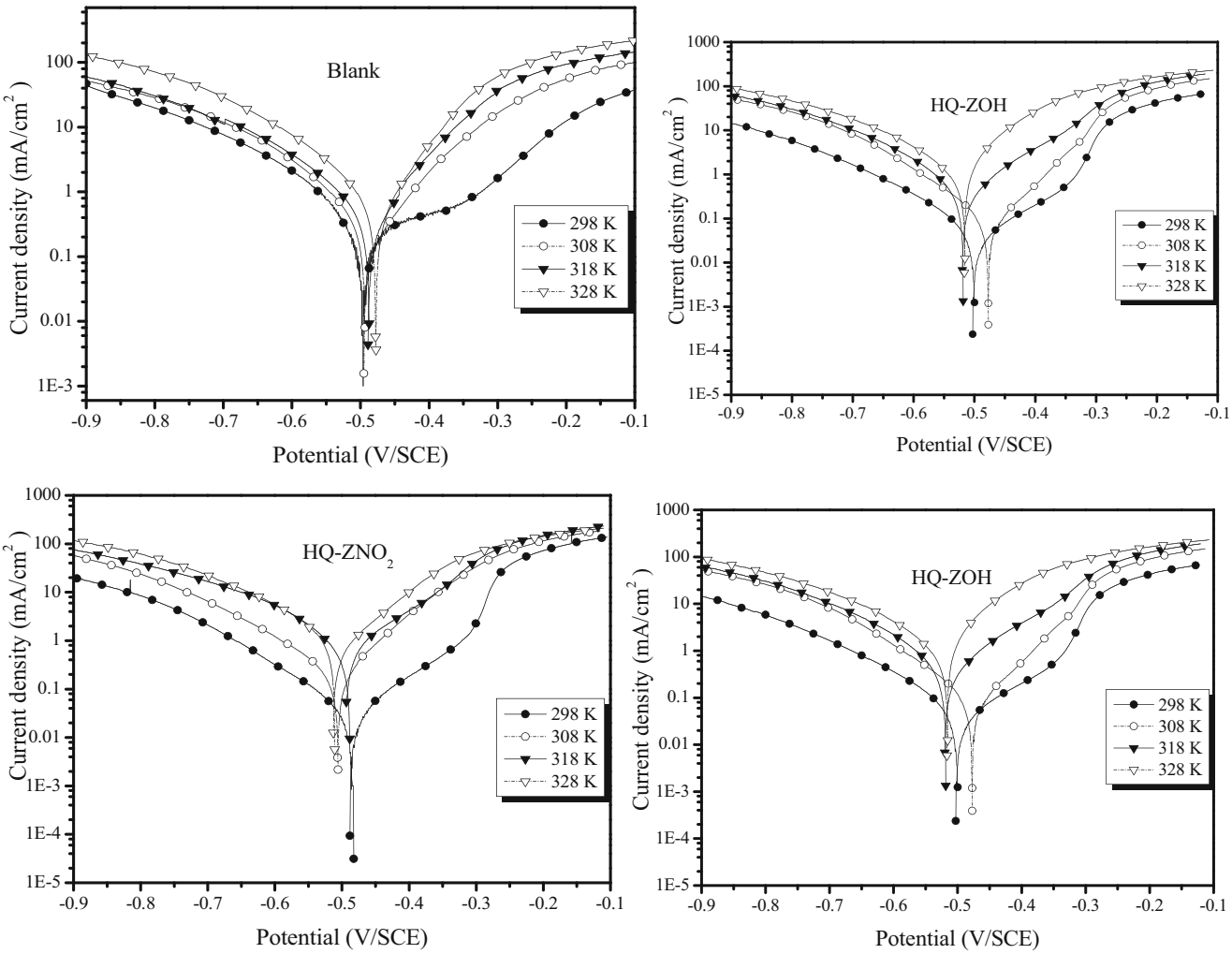

Fig. 5 Effect of temperature on the polarization curves of MS in 1 M HCl and in the presence of *HQ-ZH*, *HQ-ZNO*$_2$, and *HQ-ZOH*

Stationary electrochemical study

Concentration effect

The concentration effect of the *HQ-ZH*, *HQ-ZNO*$_2$, and *HQ-ZOH* on the polarization character for *MS* in 1 M HCl at 298 ± 2 K were analyzed. The Tafel plots were recorded at different inhibitor concentration, which is represented in Fig. 4. From Tafel plots we got the values of the anodic and cathodic Tafel slopes (β_a & β_c), corrosion current density (i_{corr}), corrosion potential (E_{corr}E$_{corr}$) and corrosion restraint effectiveness (η_{PDP} %). Table 2 shows the polarization parameters for *MS* in 1 M HCl without and with different concentrations of *HQ-ZH*, *HQ-ZNO*$_2$, and *HQ-ZOH* at 298 ± 2 K.

Analysis of the potentiodynamic polarization curves shows that the *HQ-ZH*, *HQ-ZNO*$_2$, and *HQ-ZOH* compounds decrease both the cathodic and anodic current densities, and their effect becomes more remarkable with increasing concentration. These results reveal that the *HQ-ZH*, *HQ-ZNO*$_2$, and *HQ-ZOH* compounds inhibit both anodic metal dissolution and cathodic hydrogen evolution reactions. In addition, the increase of the protective effect with the inhibitor concentration reveals that quinazoline derivatives act by adsorption on the metallic surface [37].

No definite shift was observed in the corrosion potential (E_{corr}) (Table 2). According to Riggs [38] and other authors [39], for an inhibitor of the cathodic or anodic type, the displacement should be more than 85 mV/E_{corr} while for an inhibitor of the mixed type, it is equal to or less than 85 mV/E_{corr}. In our case, the maximum displacement is < 85 mV/E_{corr}, which indicates that *HQ-ZH*, *HQ-ZNO*$_2$, and *HQ-ZOH* can be considered as a mixed-type inhibitor.

Addition of *HQ-ZH*, *HQ-ZNO*$_2$, and *HQ-ZOH* to the corrosive environment causes a modification of cathodic Tafel slope (β_c), indicating that the quinazoline derivatives have a direct influence on the kinetics of hydrogen evolution. Also, when compared corrosive environment, the values of the (β_a) changed irregularly in the presence of quinazoline derivatives, which indicates that the anodic reaction is affected by the presence of *HQ-ZH*, *HQ-ZNO*$_2$, and *HQ-ZOH*. The presence

Table 3 Values of the corrosion current density and the inhibition performance in the presence of 10^{-3} M of *HQ-ZH*, *HQ-ZNO*$_2$, and *HQ-ZOH* at different temperatures

Medium	Temp (K)	$-E_{corr}$ (mV/SCE)	i_{corr} (μA/cm^2)	$-\beta_c$ (mV dec^{-1})	β_a (mV dec^{-1})	η_{PDP} (%)
Blank	298	498	983	92	104	–
	308	491	1200	184	112	–
	318	475	1450	171	124	–
	328	465	2200	161	118	–
HQ-ZOH	298	492	84	117	112	90.8
	308	472	120	100	72	90.0
	318	514	170	87	92	88.3
	328	510	300	99	77	86.4
HQ-ZH	298	482	55	110	94	93.9
	308	470	90	142	85	92.5
	318	506	140	147	83	90.3
	328	484	235	150	78	89.3
HQ-ZNO$_2$	298	480	40	98	85	95.0
	308	502	80	106	77	93.3
	318	483	130	95	106	91.0
	328	508	220	109	85	90.0

of heteroatoms with a lone pair of electrons, such as *N* and *O* atoms in *HQ-ZH*, *HQ-ZNO*$_2$, and *HQ-ZOH* molecules can facilitate the formation of *Fe(II)- HQ-ZNO*$_2$, *Fe(II)- HQ-ZH*, and *Fe(II)- HQ-ZOH* complexes, and thus changes the dissolution mechanism of iron [40].

The polarization results are in agreement with the results of the impedance spectroscopy.

Temperature effect

The stability of a corrosion inhibitor in an aggressive medium at given use temperatures is very important for its application. In acid stripping, the role of the inhibitors is to protect the metal installations against acid attacks. These stripping operations are usually carried out at high temperatures [41]. In our case, the study of the influence of temperature (298–328 ± 2 K) on the corrosion inhibition rate of MS for the three quinazoline was carried out potentiodynamic polarization. The cathodic and anodic polarization curves of steel in 1 M HCl medium in the absence and in the presence of *HQ-ZH*, *HQ-ZNO*$_2$, and *HQ-ZOH* at 10^{-3} M are shown in Fig. 5. The values of corrosion current densities (i_{corr}), corrosion potentials of steel (E_{corr}), and the inhibitory performance of *HQ-ZH*, *HQ-ZNO*$_2$, and *HQ-ZOH* as a function of temperature are given in Table 3. We note that the increase in temperature causes an increase in i_{corr} and the inhibitory performance decreases throughout the temperature range studied [42]. It also shows that *HQ-ZH*, *HQ-ZNO*$_2$, and *HQ-ZOH* retain their inhibitory properties for all temperatures studied. However, in the case of the inhibitor *HQ-ZNO*$_2$ which proved to be the best inhibitor of this family, the decrease in the inhibitory performance is less important and reaches 90% at 328 K.

Kinetic activation parameters

The thermodynamic parameters specifically activation energy (E_{act}), entropy of activation (ΔS_{act}) and enthalpy of activation (ΔH_{act}) for corrosion reaction at 10^{-3} M for *HQ-ZNO*$_2$, were calculated from Arrhenius and transition state plot. The activation energy was calculated by Arrhenius formula:

$$i_{corr} = A\exp\left(\frac{-E_a}{RT}\right) \tag{13}$$

and other two parameters ΔH_{act} and ΔS_{act} were calculated utilizing the transition state formula:

$$i_{corr} = \frac{RT}{Nh}\exp\left(\frac{\Delta S_{act}}{R}\right)\exp\left(\frac{-\Delta H_{act}}{RT}\right) \tag{14}$$

where, *R*, *T*, *A*, *N*, and *h* are universal gas constant, absolute temperature, pre-exponential factor, Avogadro number and plank constant, respectively. The i_{corr} values were obtained from the extrapolation of Tafel plot at different temperature with and without adding *HQ-ZH*, *HQ-ZNO*$_2$, and *HQ-ZOH* molecules. Here, i_{corr} values consider as a corrosion rate. From the Arrhenius plots, Ln i_{corr} against 1000/*T* at optimum concentration of *HQ-ZNO*$_2$, *HQ-ZH* and *HQ-ZOH* display in Fig. 6.

According to Fig. 6, showing a straight line curve having a slope equal to $-E_a/RT$ and E_a was calculated from this slope. Another plot of Ln (i_{corr} /*T*) vs. 1000/*T* show a straight line

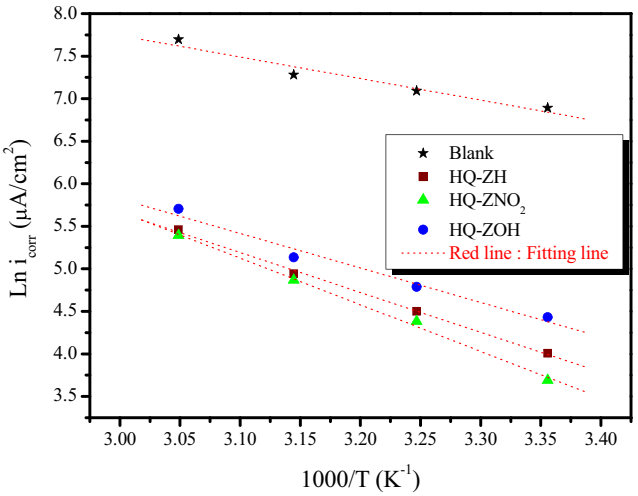

Fig. 6 Arrhenius plots for MS corrosion in 1 M HCl in the absence and presence of *HQ-ZH*, *HQ-ZNO*$_2$, and *HQ-ZOH*

curve (Fig. 7) with a slope and intercept those are equal to $-\Delta H_{act}$ /R and Ln $(R/Nh) + \Delta S_{act}/R$, respectively.

The values of ΔH_{act} and ΔS_{act} listed in Table 4 which were calculated from the slope and intercept. From Table 4 and Fig. 6, it can be seen that the activation energy (E_{act}) in presence of three *HQ-ZH*, *HQ-ZNO*$_2$, and *HQ-ZOH* is higher than the blank solution on *MS* corrosion which indicates the metal dissolution decreases in acidic medium because of increase in the energy barrier for *MS* corrosion. In 1965 Radovici proposes that when E_{act} (inh) > E_{act} (blank), inhibitors adsorbs on the substrate by electrostatic nature bonds (weak bonds). The results obtained in Table 5 indicate that the increase in activation energy in the presence of the studied inhibitors can be attributed to the phenomenon of physisorption. The bonds formed in this type of interaction can be sensitive to temperature and does not allow fighting effectively against corrosion when the temperature increases.

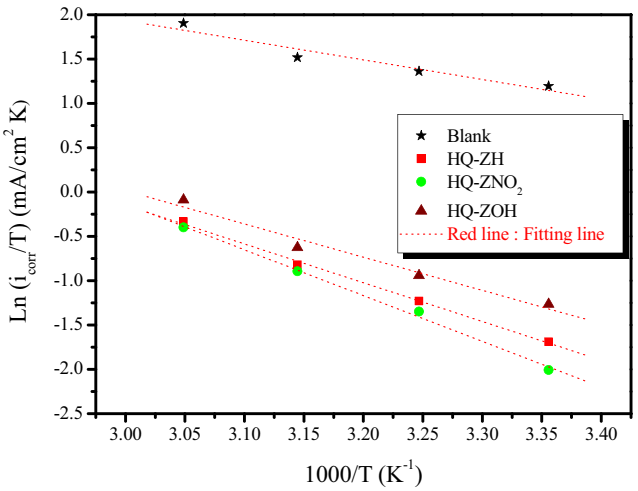

Fig. 7 Transition state plots for *HQ-ZH*, *HQ-ZNO*$_2$, and *HQ-ZOH* in 1 M HCl medium on MS corrosion

Table 4 Activation parameters of *MS* corrosion in 1 M HCl medium without and with addition of three *HQ-ZH*, *HQ-ZNO*$_2$, and *HQ-ZOH* at 10^{-3} M

Medium	E_a (KJ mol^{-1})	ΔH_a (KJ mol^{-1})	$-\Delta S_a$ (J mol^{-1} K^{-1})
Blank	21.00	18.50	126.0
HQ-ZOH	33.73	31.14	104.0
HQ-ZH	38.96	36.36	89.69
HQ-ZNO$_2$	45.56	42.96	69.75

Meanwhile, the activation entropy (ΔS_{act}) value increases in addition of *HQ-ZH*, *HQ-ZNO*$_2$, and *HQ-ZOH* compared to given acid solution and the values were found in negative. The higher ΔS_{act} values in presence of *HQ-ZH*, *HQ-ZNO*$_2$, and *HQ-ZOH* signified the entropy of the solvent increases. This may occur due to desorption of large numbers of water molecule which were already adsorbed on the metal surface and less disorder larger *HQ-ZH*, *HQ-ZNO*$_2$, and *HQ-ZOH* molecules adsorbed on the MS surface [43, 44].

Isotherms and thermodynamic parameters of adsorption

The adsorption isotherm provides some useful information regarding corrosion mechanism. Many factors control the adsorption process, like nature of the metal surface and its charge, solvent, and other ionic species adsorption, electrochemical potential between metal-solution interface, temperature during corrosion reaction. The adsorption process is divided into two categories. First one is chemisorption; it occurs when the direct interaction between adsorbed inhibitors molecule and metal surface like donor-accepter type interaction. Chemical adsorption implies the charge sharing or charge transfer from adsorbates (inhibitor molecule) to the metal surface and forms a very strong metal-inhibitor coordinate bond. This types of interaction are basically irreversible in nature. The second one is physisorption; here, the inhibitor molecules adsorb on the metal surface through week undirected interaction which is basically formed due to the electrostatic interaction between metal and inhibitor's solution interface [45]. To evaluate the adsorption isotherm nature, several adsorption isotherms were tested. It was observed that the adsorption of *HQ-ZH*, *HQ-ZNO*$_2$, and *HQ-ZOH* on MS in 1 M HCl medium obey the Langmuir adsorption isotherm formula:

$$\frac{C_{inh}}{\theta} = \frac{1}{K_{ads}} + C_{inh} \tag{15}$$

where K_{ads}, θ and C_{inh} are inhibitor adsorption constant, degree of surface coverage, and *HQ-ZH*, *HQ-ZNO*$_2$, and *HQ-ZOH* concentration, respectively. Values of $\theta = \eta/100$ were taken from polarization measurement. The plot of C_{inh}/θ vs

Table 5 Activation parameters of MS corrosion in 1 M HCl medium without and with addition of *HQ-ZH*, *HQ-ZNO*$_2$, and *HQ-ZOH* at 10^{-3} M

Inhibitors	K_{ads} (L mol^{-1})	R^2	$-\Delta G^{\circ}_{ads}$ (KJ mol^{-1})
HQ-ZOH	2,481,789.87	1	46.43
HQ-ZH	844,608.86	1	43.76
HQ-ZNO$_2$	656,331.63	1	43.14

C_{inh} gave a straight line curve (Fig. 8) having $1/K_{ads}$ intercept and the correlation coefficient (R^2) value for three *HQ-ZH*, *HQ-ZNO*$_2$, and *HQ-ZOH* is 1.00.

The straight line and strong correlation coefficient value indicate the Langmuir adsorption isotherm the best fitted with experimental data. The ΔG^{o}_{ads} value was calculated utilizing the formula:

$$\Delta G^{\circ}_{ads} = -RTLn(55.55K_{ads}) \quad (16)$$

where, T is the temperature, R is the gas constant. The values of K_{ads} is represented here in L mol^{-1}, thus in this formula the conc. of water is taken in L mol^{-1} (55.5 mol/L). In general when the obtained ΔG^{o}_{ads} values of inhibitor lie in the order of − 20 kJ mol^{-1} or even lower (more positive), it satisfies the physisorption of inhibitor on metal surface. While the ΔG^{o}_{ads} values around − 40 kJ mol^{-1} or higher (more negative) are associated with chemisorption [46]. The obtained ΔG^{o}_{ads} values of *HQ-ZH*, *HQ-ZNO*$_2$, and *HQ-ZOH* are − 46.43 kJ/mol, − 43.76 kJ/mol, and − 43.14 kJ/mol for *HQ-ZH*, *HQ-ZNO*$_2$, and *HQ-ZOH*, respectively (Table 6). The above range of ΔG^{o}_{ads} values indicates the contribution of chemisorption [47].

UV-visible spectroscopy

The absorption of monochromatic light is a suitable method for identification of complex ions, the absorption of light is proportional to the concentration of the absorbing species. For routine analysis, a simple conventional technique based on UV–vis absorption is the more sensitive direct spectrophotometric detection. Change in position of the absorption maximum and or change in the value of absorbance indicate the formation of a complex between two species in solution.

To better understand the binding mechanism between inhibitors and iron in the acid solution, we use UV-visible spectroscopy. The electron absorption spectra of HQ-ZNO$_2$, *HQ-ZH* and *HQ-ZOH* solutions Fig. 9, before immersion of MS in 1 M HCl solution show visible absorption bands 251.93, 251.92, and 254.42 nm. respectively for *HQ-ZNO*$_2$, *HQ-ZH*, and *HQ-ZOH*. This band may be assigned to the $\pi - \pi^*$ transition involving the whole electronic structure system of the substituted quinazoline compound with a considerable charge transfer character [10, 48].

However, after 24 h of immersion of specimen in aggressive solution Fig. 8, the absorption bands λ_{max} underwent a bathochromic shift from 251.93 at 257.92 nm, 251.92 at 254.93 nm, and 254.42 at 260.77 nm, respectively for *HQ-ZNO*$_2$, *HQ-ZH*, and *HQ-ZOH*. Our experimental findings are good evidence for the possibility of the formation of a complex among Fe^{2+} and inhibitors in HCl 1 M.

Surface morphology

Scanning electron micrographs (Fig. 10) of the mild steel surface in 1 M HCl with and without addition of *HQ-ZNO*$_2$, *HQ-ZOH*, and *HQ-OH* were taken in order to establish whether inhibition is due to the formation of an organic film on the metal surface. The resulting of the high-resolution SEM micrograph shows that the steel surface was strongly damaged in the absence of the three

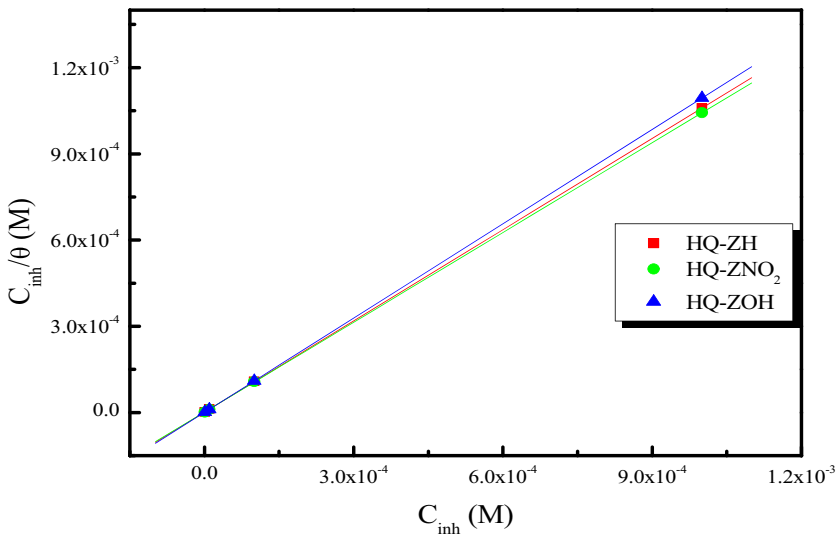

Fig. 8 Langmuir adsorption isotherm plots for the adsorption of *HQ-ZH*, *HQ-ZNO*$_2$, and *HQ-ZOH* on MS corrosion surface in 1 M hydrochloric acid

Table 6 Calculated quantum chemical parameters of the studied compounds

Parameters	*HQ-ZH*	*HQ-ZOH*	*HQ-ZNO$_2$*
E_{LUMO} *(eV)*	− 1.469	− 1.415	− 1.721
E_{HOMO} *(eV)*	− 5.687	− 5.660	− 4.905
ΔE *(eV)*	4.218	4.245	3.184
μ (debyes)	1.500	1.780	5.440
η *(eV)*	2.109	2.122	1.590
σ *(eV^{-1})*	0.474	0.471	0.628
Pi (eV)	− 3.570	− 3.540	− 3.313
χ *(eV)*	3.570	3.540	3.313
A (eV)	1.469	1.415	1.721
ΔN *(eV)*	0.813	0.815	1.157
TE (u.a)	− 1239.500	− 1314.780	− 1444.060

inhibitors with the increased number and depth of the pits. However, there are less pits and cracks observed in the micrographs in the presence of *HQ-ZNO$_2$, HQ-ZOH*, and *HQ-OH* (Fig. 10) which suggests a formation of protective film on steel surface which was responsible for the corrosion inhibition. Indeed, *HQ-ZNO$_2$*, *HQ-ZOH*, and *HQ-OH* has a strong tendency to adhere to the steel surface and can be regarded as good inhibitors for steel corrosion in normal hydrochloric medium. The high inhibitive performance of these quinazoline derivatives suggests a strong bonding of the *HQ-ZNO$_2$, HQ-ZOH*, and *HQ-OH* on the metal surface due to presence of lone pairs from heteroatom (nitrogen and oxygen) and π-orbitals, blocking the active sites and therefore decreasing the corrosion rate.

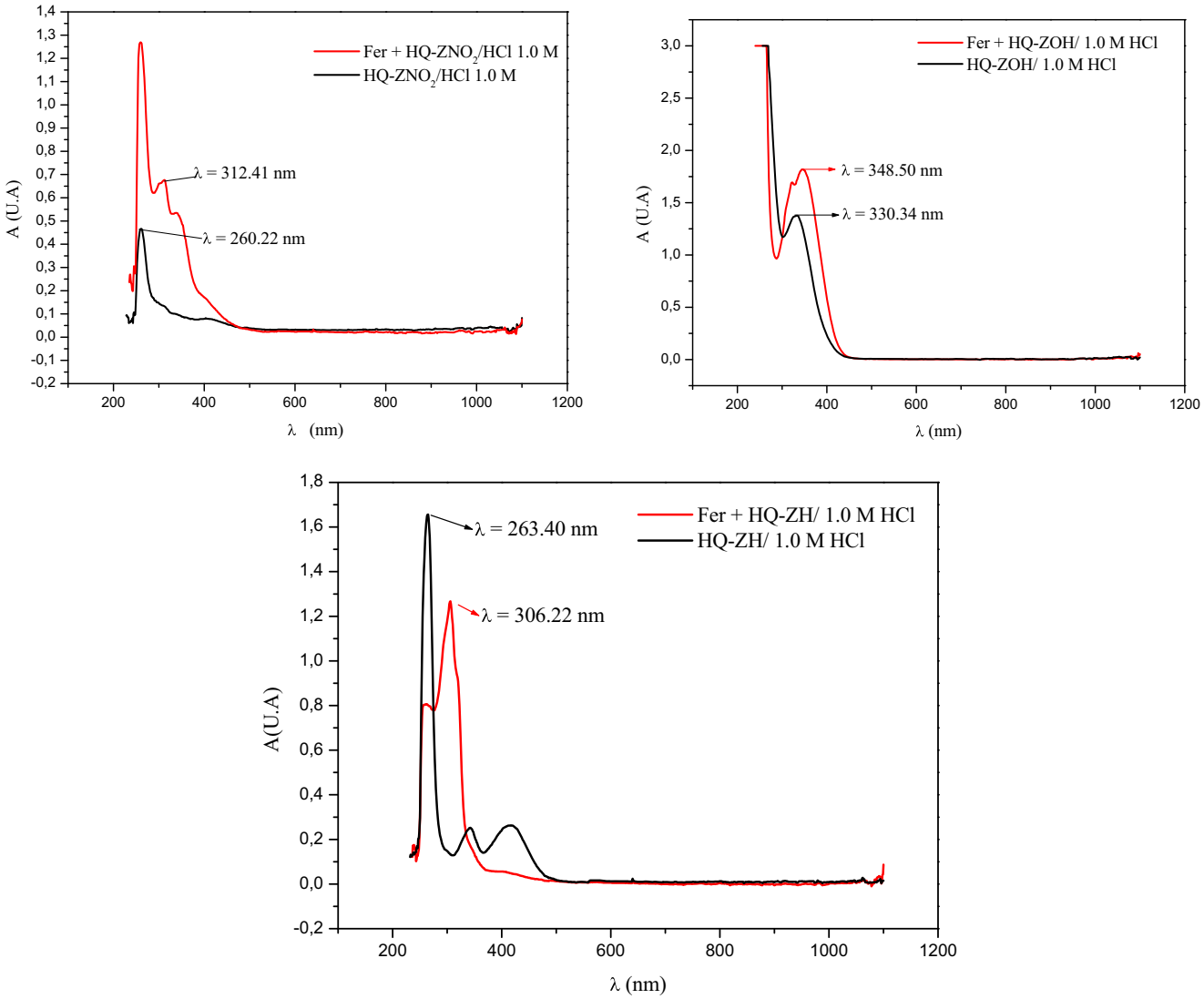

Fig. 9 UV-visible spectra of 1 M HCl solution containing 10^{-3} M of *HQ-ZNO$_2$, HQ-ZOH*, and *HQ-OH* before (black) and after (red) After 24 h of MS immersion

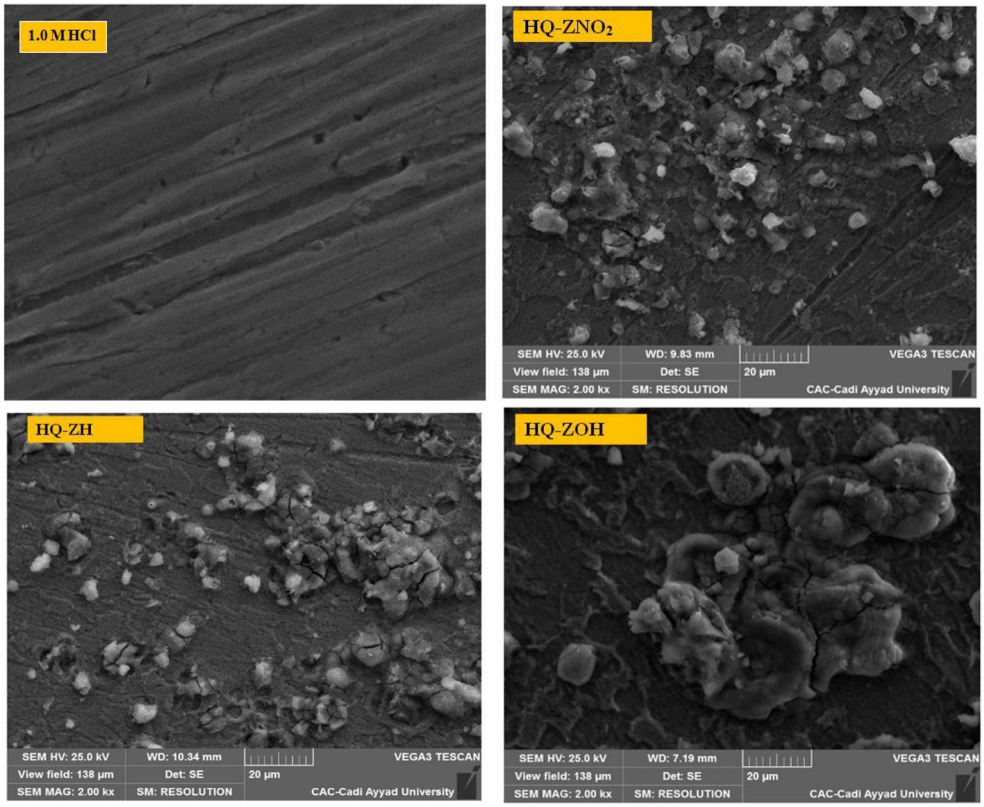

Fig. 10 Surface morphology of *MS* before and after immersion for 6 h in 1 M HCl with 1 mM of *HQ-ZNO$_2$*, *HQ-ZOH*, and *HQ-ZOH*

Theoretical calculations

Density functional theory

Frontier molecular orbitals To obtain detailed information about the mechanism of inhibition, quantum theoretical calculation by the *DFT 6–31 G (d,p)* methods were carried out and compared with the experimental results. For this, we performed a theoretical calculation to determine the quantum chemical parameters, such as highest occupied molecular orbital energy (E_{HOMO}), lowest unoccupied molecular orbital energy (E_{LUMO}), energy gap (ΔE), dipole moment (μ) etc.

The energy (E_{HOMO}) indicates the ability of the molecule to yield electrons to another empty molecular orbit, but the value of E_{LUMO} energy describes the ability of a compound to accept electrons. The energy difference between (E_{HOMO}) and (E_{LUMO}) or energy gap is generally the lowest electronic energy excitation. The adsorption of energy between the metal surface of iron and the inhibitors increases once the gap energy decreases [49].

The optimized geometry of the structure, its *HOMO* and *LUMO* electron density distributions are given in Fig. 11.

The analysis of Fig. 11 shows that the electronic density for the three inhibitors, *HOMO* is distributed on the cycle quinoline.

The *LUMO* electronic density is localized on the ring substituted by *-NO$_2$* for *HQ-ZNO$_2$*. However, for compounds *HQ-ZH* and *HQ-ZOH*, the *LUMO* is distributed throughout the cycle quinoline.

Frontier molecular orbital energies The values of calculated quantum chemical parameters are listed in Table 6. The higher the (*HOMO*) energy of the inhibitor, the greater the trend of offering electrons to unoccupied (*d*) orbital of the metal, the lower the (*LUMO*) energy, The process of transition of electrons to the metal surface is easy, the analysis of Table 6 shows that the highest value of E_{HOMO} (− 4.905 eV) of *HQ-ZNO$_2$* indicates a better inhibition performance than E_{HOMO} (− 5.687 eV) of *HQ-ZH* and E_{HOMO} (− 5.660 eV) of *HQ-ZOH*. The lower the E_{LUMO}, the easier is the acceptance of electrons from the d-orbital of the metal. The lowest value of E_{LUMO} (− 1.721 eV) of *HQ-ZNO$_2$* indicates a better inhibition performance in this family.

Low values of the energy of the gap $\Delta E = E_{LUMO} - E_{HOMO}$ implies that the energy to remove an electron from the last occupied orbital will be minimized, corresponding to improved inhibition efficiencies. The values of the gap energy are listed in Table 6. We notice that the values of the ΔE for the compounds tested *HQ-ZNO$_2$*, *HQ-ZOH*, and *HQ-OH* are 3.184 eV, 4.218 eV, and 4.245 eV, respectively.

The quality of inhibition by the *HQ-ZNO$_2$* compound is higher than *HQ-ZOH* and *HQ-ZH*.

We classify these derivatives according to their energies of gape:

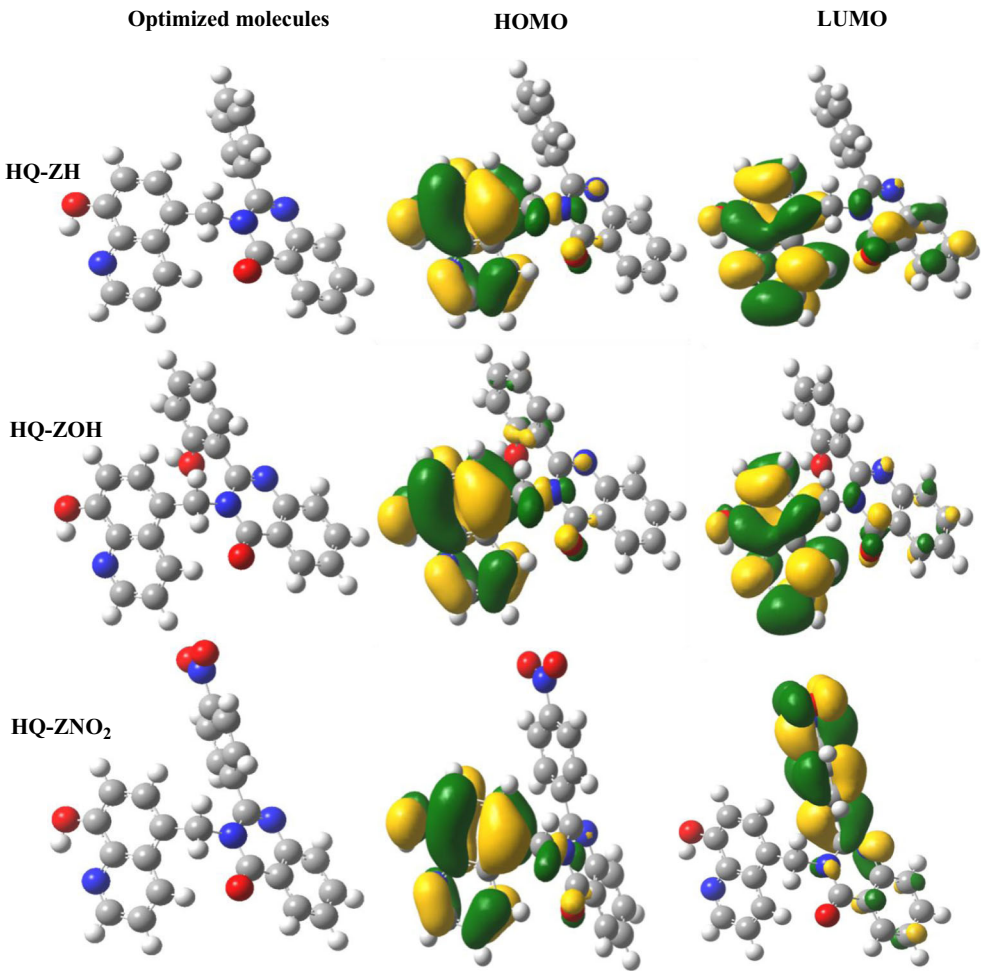

Fig. 11 Optimized structure and Frontier molecular orbital's neutral of inhibitors molecules

$$\Delta E(HQ{-}ZOH) > \Delta E(HQ{-}ZH) > \Delta E(HQ{-}ZNO_2)$$

The results obtained in Table 6 indicate that the effectiveness of inhibition of inhibitors tested increased with the ionization potential (Pi); the *HQ-ZNO₂* compound has the highest ionization potential (− 3.313 eV).

Chemical hardness (η) and softness (σ) are important properties to measure the molecular stability and reactivity. The values calculated of (σ) and (η) are also listed in Table 6. The compound *HQ-ZNO₂* has a good reactivity chemical to the surface of Metal due to the increase of the value of softness ($\sigma = 0.628\ eV^{-1}$) and the diminution of hardness ($\eta = 1.590$ eV).

The fraction of electrons transferred (ΔN) from inhibitor to *MS* surface was also calculated utilizing a theoretical χ_{Fe} and η_{Fe} values for MS. The total energy of the best inhibitor *HQ-ZNO₂* is the lowest among the compounds studied; this result indicates that the *HQ-ZNO₂* is well adsorbed on the metal surface. The inhibitory performance increases with the increase of the electron donor of the inhibitor on the surface of the metal (ΔN). The compound *HQ-ZNO₂* has a high value of ΔN (1.157 eV) in the order of ΔN *(HQ-ZNO₂)* > ΔN *(HQ-ZH)* ≈ ΔN *(HQ-ZOH)*.

These results agree with the experimental observations, which imply that *HQ-ZNO₂* compound has better corrosion performance.

Fukui index analysis The importance of the highest occupied molecular orbital and the lowest unoccupied molecular orbital in chemical reactions was introduced and explained by Fukui. Since a chemical reaction is nothing other than an exchange of electrons between reagents, we can understand the importance of the Fukui hypothesis, which gives an insight into molecular reactivity.

The electrophilic and nucleophilic chemical reactivity of the atoms for the three quinoline compounds is listed in Table 7, which contains the values of the natural population [*(P (N), P (N–1)* and *P (N + 1)*] with the corresponding values of the Fukui functions (f_k^- and f_k^+) of the studied molecules. The *C27* atom, which belongs to two 8-hydroxyquinoline moiety, is available for electrophilic attack for all three compounds. The *C1*, *C24*, and *C28* atoms of compound *HQ-ZH* possess a high value of the Fukui function; moreover, they are available for nucleophilic attack.

Table 7 Values of the Fukui function considering natural population analysis (*NPA*) of molecules calculated at the *$B_3LYP/6–31\ G\ (d, p)$*

Inhibitors	Atoms	*P(N)*	*P (N+ 1)*	*P (N-1)*	f_k^+	f_k^-
HQ-ZH	C1	5.389	5.315	5.316	− 0.074	0.073
	C2	6.159	6.164	6.210	0.005	− 0.051
	C3	5.809	5.821	5.848	0.012	− 0.039
	C4	5.526	5.510	5.588	− 0.016	− 0.062
	C6	6.172	6.167	6.184	− 0.005	− 0.012
	C7	6.240	6.192	6.236	− 0.048	0.004
	C8	6.209	6.205	6.251	− 0.004	− 0.042
	C9	6.244	6.192	6.296	− 0.052	− 0.052
	C24	6.435	6.297	6.278	− 0.138	0.157
	C27	6.003	5.965	6.094	− 0.038	− 0.091
	C28	6.078	6.085	6.067	0.007	0.011
	C29	6.262	6.187	6.228	− 0.075	0.034
	C30	6.174	6.152	6.234	− 0.022	− 0.06
	C31	5.861	5.864	5.878	0.003	− 0.017
	C32	6.265	6.243	6.316	− 0.022	− 0.051
	C34	6.271	6.245	6.296	− 0.026	− 0.025
	C36	5.685	5.586	5.669	− 0.099	0.016
	C38	5.966	5.927	6.007	− 0.039	− 0.041
	O41	8.665	8.586	8.665	− 0.079	0
	N42	7.492	7.432	7.518	− 0.06	− 0.026
	N43	7.376	7.436	7.460	0.06	− 0.084
	O44	8.717	8.604	8.706	− 0.113	0.011
	N46	7.449	7.462	7.544	0.013	−0.095
$HQ\text{-}ZNO_2$	C1	5.316	5.315	5.316	− 0.001	0
	C2	6.167	6.166	6.190	− 0.001	−0.023
	C3	5.830	5.821	5.827	− 0.009	0.003
	C4	5.527	5.518	5.549	− 0.009	−0.022
	C6	6.183	6.166	6.187	− 0.017	−0.004
	C7	6.224	6.192	6.242	− 0.032	−0.018
	C8	6.212	6.202	6.225	− 0.01	−0.013
	C9	6.238	6.192	6.282	− 0.046	−0.044
	C26	6.083	5.956	6.078	− 0.127	0.005
	C27	6.069	6.086	6.067	0.017	0.002
	C28	6.199	6.189	6.190	− 0.01	0.009
	C29	6.179	6.150	6.189	− 0.029	− 0.01
	C30	5.874	5.864	5.879	− 0.01	− 0.005
	C31	6.301	6.233	6.301	− 0.068	0
	C33	6.300	6.241	6.295	− 0.059	0.005
	C37	5.958	5.925	5.973	− 0.033	− 0.015
	O40	8.629	8.582	8.658	− 0.047	− 0.029
	N41	7.480	7.433	7.515	− 0.047	− 0.035
	N42	7.449	7.436	7.453	− 0.013	− 0.004
	N45	7.487	7.458	7.507	− 0.029	− 0.020
	O43	8.683	8.593	8.697	− 0.09	− 0.014
HQ-ZOH	C1	5.317	5.316	5.368	− 0.001	− 0.051
	C2	6.169	6.165	6.161	− 0.004	0.008
	C3	5.825	5.821	5.824	− 0.004	0.001
	C4	5.515	5.511	5.527	− 0.004	− 0.012
	C6	6.184	6.170	6.237	− 0.014	− 0.053

Table 7 (continued)

Inhibitors	Atoms	*P(N)*	*P (N+ 1)*	*P (N-1)*	f_k^+	f_k^-
	C7	6.226	6.197	6.273	− 0.029	− 0.047
	C8	6.215	6.204	6.254	− 0.011	− 0.039
	C9	6.244	6.199	6.258	− 0.045	− 0.014
	C26	6.078	5.960	6.112	− 0.118	− 0.034
	C27	6.067	6.083	6.056	0.016	0.011
	C28	6.197	6.190	6.236	− 0.007	− 0.039
	C29	6.177	6.148	6.261	− 0.029	− 0.084
	C30	5.873	5.863	5.877	− 0.01	− 0.004
	C31	6.299	6.255	6.330	− 0.044	− 0.031
	C33	6.278	6.246	6.308	− 0.032	− 0.03
	C35	5.645	5.591	5.697	− 0.054	− 0.052
	C37	5.960	5.927	6.003	− 0.033	− 0.043
	O40	8.636	8.595	8.674	− 0.041	− 0.038
	N41	7.470	7.431	7.515	− 0.039	− 0.045
	N42	7.448	7.433	7.438	− 0.015	0.010
	O33	8.687	8.610	8.721	− 0.077	− 0.034
	N45	7.489	7.465	7.567	− 0.024	− 0.078

The atoms *C3*, *C26*, and *C28* of compound *HQ-ZNO*$_2$ possess a high value of the function of Fukui; these atoms are considered as sites available for electrons (nucleophilic attack). The *C2*, *C3*, and *C27* atoms of compound *HQ-ZOH* possess a high value of the function of Fukui; these atoms are available for electrophilic attack.

Monte Carlo simulations

Monte Carlo simulations were carried out to simulate the low energy adsorption configuration and to determine the adsorption energies as the inhibitor molecules slowly interacts with Fe surface. This methodology has earlier been adopted by us to understand the strength and mechanism of inhibitor-metal interactions in the literature [50, 51].

As can be seen in Fig. 12(a–c), the three inhibitor molecules (*HQ-ZNO*$_2$, *HQ-ZOH*, and *HQ-OH*) are adsorbed in a parallel orientation to the metal surface to maximize contact. The heteroatoms such as *N* and *O* present in the molecules were in close contact with the Fe surface and could serve as the adsorption sites. Although *NO*$_2$,-group is an electron withdrawing group, the presence of extra O atom in *HQ-NO*$_2$

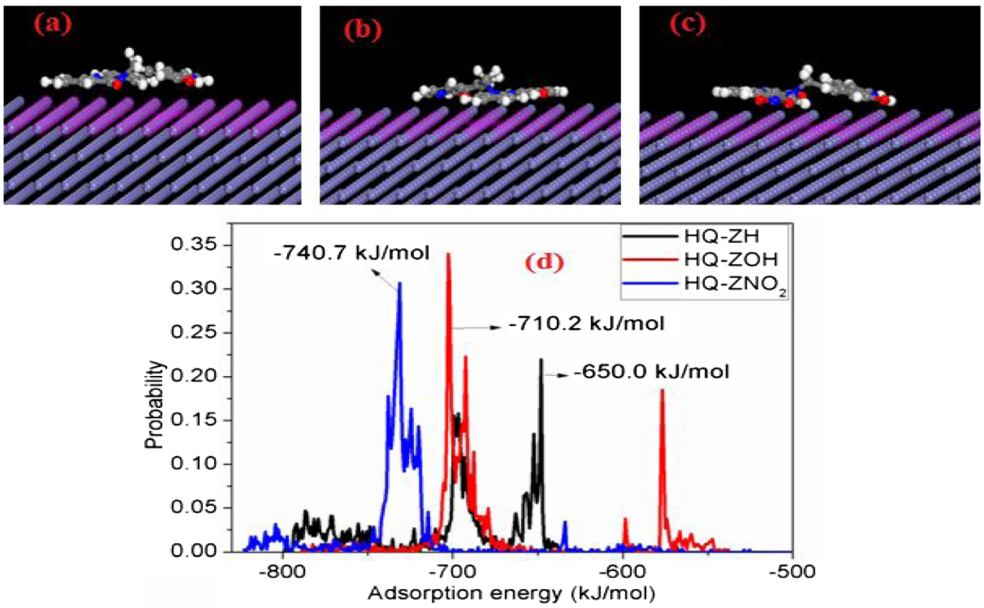

Fig. 12 Model Structures simulating the equilibrium adsorption configuration of (**a**) *HQ-ZH*, (**b**) *HQ-ZOH* and (**c**) *HQ-ZNO*$_2$ on the Fe surface. (**d**) Probability distribution curves in adsorption energy function for *HQ-ZH*, *HQ-ZOH*, and *HQ-ZNO*$_2$ on the Fe surface

could enhance its interaction with Fe surface when compared with other inhibitors investigated. This could result in a higher adsorption energy for *HQ-NO₂*. Figure 11d shows the probability distribution curves for the adsorption energies of the three inhibitors on the Fe surface. It can be seen that *HQ-NO₂* has a higher negative adsorption energy when compared to *HQ-ZH*, *HQ-ZOH*, which suggests a stronger interaction of the inhibitor molecule with the metal surface [52]. In fact, the order of the adsorption energy is *HQ-ZNO₂* > *HQ-ZOH* > *HQ-ZH*. We conclude from the results obtained that the interaction between *HQ-ZNO₂* and the steel surface is greater than that of the other two inhibitor molecules studied. This result indicates that is *HQ-ZNO₂* is expected to inhibit steel corrosion more than *HQ-ZH* and *HQ-ZOH*. The results obtained utilizing Monte Carlo simulations are in good agreement with the experimentally determined corrosion inhibition efficiencies of the three molecules investigated.

Conclusion

The inhibition effect and adsorption behavior of the quinazolinone derivatives have been investigated utilizing electrochemical studies, *SEM* surface investigations, *UV−vis* and quantum chemical calculations. The conclusions of these investigations are as follows:

- Quinazolinone derivatives acted as efficient corrosion inhibitors for MS in acidic medium.
- Polarization studies have shown that the studied inhibitors acting as mixed inhibitors.
- EIS study revealed that values of polarization resistance (R_p) increase in presence of inhibitors due to the adsorption of inhibitors at metal/electrolyte interfaces.
- The adsorption of the inhibitors on the MS surface obeys the Langmuir adsorption isotherm.
- The adsorption of quinazoline compounds was investigated by using UV-visible, *SEM* techniques.
- *DFT* and Monte Carlo simulations support the experimental outcomes.

Acknowledgments I.B. Obot is grateful to King Fahd University of Petroleum and Minerals, (KFUPM) Saudi Arabia, and the Centre of High Performance Computing (KFUPM) for making the computational software available for this work. We thank also the "National Center for Scientific and Technical Research" and the "Moroccan Ministry of Higher Education" for providing all the facilities and for supporting this work.

References

1. Bagga MK, Gadi R, Yadav OS, Kumar R, Chopra R, Singh G (2016) Investigation of phytochemical components and corrosion inhibition property of Ficus racemosa stem extract on mild steel in H2SO4 medium. J Environ Chem Eng 4:4699–4707
2. Hassan KH, Khadom AA, Kurshed NH, (2016) Citrus aurantium leaves extracts as a sustainable corrosion inhibitor of mild steel in sulfuric acid. South African J Chem Eng 22: 1–5
3. Amin MA, Abd El-Rehim SS, El-Sherbini EEF, Bayoumi RS (2007) The inhibition of low carbon steel corrosion in hydrochloric acid solutions by succinic acid. Electrochim Acta 52:3588–3600
4. Garai S, Garai S, Jaisankar P, Singh JK, Elango A (2012) A comprehensive study on crude methanolic extract of Artemisia pallens (Asteraceae) and its active component as effective corrosion inhibitors of mild steel in acid solution. Corros Sci 60:193–204
5. Dupin P, De Savignac A, Lattes A (1981) Influence des "concentrations critiques d'agregation" sur le comportement inhibiteur de corrosion d'imidazoles et imidazolines substitues. J Mater Chem 6(6):443–453
6. Zarrouk A, Zarrok H, Salghi R, Touir R, Hammouti B, Benchat N, Afrine LL, Hannache H, El Hezzat M, Bouachrine M (2013) Electrochemical impedance spectroscopy weight loss and quantum chemical study of new pyridazine derivative as inhibitor corrosion of copper in nitric acid. J Chem Pharm Res 5(12):1482–1491
7. Zarrok H, Salghi R, Zarrouk A, Hammouti B, Oudda H, Bazzi Lh, Bammou L, Al-Deyab SS (2012) Investigation of the Inhibition Effect of N-1-Naphthylethylenediamine Dihydrochloride Monomethanolate on the C38 Steel Corrosion in 0.5M H2SO4. Der Pharma Chem 4(1):407–416
8. Tayebi H, Bourazmi H, Himmi B, El Assyry A, Ramli Y, Zarrouk A, Geunbour A, Hammouti B (2014) Combined electrochemical and quantum chemical study of new quinoxaline derivative as corrosion inhibitor for carbon steel in acidic media. Der Pharma Chem 6(5):220–234
9. Tayebi H, Bourazmi H, Himmi B, El Assyry A, Ramli Y, Zarrouk A, Geunbour A, Hammouti B, Ebenso EE (2014) An electrochemical and theoretical evaluation of new quinoline derivative as a corrosion inhibitor for carbon steel in HCl solutions. Der Pharm Lett 6(6):20–34
10. Abboud Y, Abourriche A, Saffaj T, Berrada M, Charrouf M, Bennamara A, Hannache H (2007) 2,3-Quinoxalinedione as a novel corrosion inhibitor for mild steel in 1M HCl. Mater Chem Phys 105(1):1–5
11. Galai M, Rbaa M, El Kacimi Y, Ouakki M, Dkhirech N (2017) Anti-corrosion Properties of some Triphenylimidazole Substituted Compounds in Corrosion Inhibition of Carbon Steel in 1.0 M Hydrochloric Acid Solution. Anal Bioanal Chem 9:80–101
12. Hmamou DB, Salghi R, Zarrouk A, Hammouti B, Al-Deyab SS, Zarrok H, Bazzi L (2012) Corrosion Inhibition of Steel in 1 M Hydrochloric Acid Medium by Chamomile Essential Oils. Int J Electrochem Sci 7:2361–2373
13. Zarrouk A, Hammouti B, Dafali A, Bentiss F (2013) Inhibitive properties and adsorption of purpald as a corrosion inhibitor for copper in nitric acid medium. Ind Eng Chem Res 52(7):2560–2568
14. Rbaa M, Galai M, El Kacimi Y, Ouakki M, Touir R (2017) Adsorption properties and inhibition of carbon steel corrosion in a hydrochloric solution by 2-(4,5-diphenyl-4,5-dihydro-1h-imidazol-2-yl)-5-methoxyphenol. Port Electrochim Acta 35(6):323–338
15. Rbaa M, Galai M, El Faydy M, El Kacimi Y, Ebn Touhami M, Zarrouk A, Lakhrissi B (2017) Synthesis and characterization of new benzimidazoles derivatives of 8-hydroxyquinoline as a

corrosion inhibitor for mild steel in 1.0 M hydrochloric acid medium. Anal Bioanal Electrochem 9(7):904–928
16. Hmamou DB, Salghi R, Zarrouk A, Zarrouk H, Errami M, Hammouti B, Bazzi L (2013) Adsorption and corrosion inhibition of mild steel in hydrochloric acid solution by verbena essential oil. Res Chem Intermed 39(3):973–989
17. Hedayatullah M, Lion C, Tourki A (1993) Nouveaux Décontaminants. Destruction Chimique du Paraoxon Et du Parathion au Moyen de Composés a Chlore Positif. Bull Soc Chim Belg 102(4):281–291
18. Rbaa M, Galai M, El Faydy M, El Kacimi Y, Ebn Touhami M, Zarrouk A, Lakhrissi B (2017) Synthesis, inhibition effects and thermodynamic studies of novel substituted quinolines on the corrosion of mild steel in 1 M HCl solution. J Mater Environ Sci 8(10): 3529–3549
19. Popova A, Christov M, Raicheva S, Sokolova E (2004) Adsorption and inhibitive properties of benzimidazole derivatives in acid mild steel corrosion. Corros Sci 46(6):1333–1350
20. Ayati NS, Khandandel S, Momeni M, Moayed MH, Davoodi A, Rahimizadeh M (2011) Inhibitive effect of synthesized 2-(3-pyridyl)-3,4-dihydro-4-quinazolinone as a corrosion inhibitor for mild steel in hydrochloric acid. Mater Chem Phys 126(3):873–879
21. Saha SK, Murmu M, Murmu NC, Banerjee P (2016) Evaluating electronic structure of quinazolinone and pyrimidinone molecules for its corrosion inhibition effectiveness on target specific mild steel in the acidic medium: a combined DFT and MD simulation study. J Mol Liq 224:629–638
22. Karnakar K, Kumar AV, Murthy SN, Ramesh K, Nageswar YVD (2012) Recyclable graphite oxide promoted efficient synthesis of 2-phenyl quinazoline derivatives in the presence of TBHP as an oxidant. Tetrahedron Lett 53(34):4613–4617
23. Rbaa M, Errahmany N, El Kacimi Y, Galai M, El Fayrdy M, Lakhrissi B, Touhami M, Lakhrissi B (2018) Chemical and electrochemical studies of novel quinazolinone derivatives based on 8-hydroxyquinoline as corrosion inhibitor for mild steel in 1.0 M HCl solution. Anal Bioanal Electrochem 10(10):1328–1354
24. El Faydy M, Galai M, Rbaa M, Ouakki M, Lakhrissi B, Touhami ME, El Kacimi Y (2018) Synthesis and application of new quinoline as hydrochloric acid corrosion inhibitor of carbon steel. Anal Bioanal Electrochem 10(7):815–839
25. Hashim NM, Rahim AA, Osman H, Raja PB (2012) Quinazolinone compounds as corrosion inhibitors for mild steel in sulfuric acid medium. Chem Eng Commun 199(6):751–766
26. Fouda AS, El-desoky AM, Hassan HM (2013) Quinazoline Derivatives as Green Corrosion Inhibitors for Carbon Steel in Hydrochloric Acid Solutions. Int J Electrochem Sci 8:5866–5885
27. Rbaa M, Galai M, El Faydy M, Lakhrissi Y, EbnTouhami M, Zarrouk A, Lakhrissi B (2018) Synthesis and characterization of new quinoxaline derivatives of 8-hydroxyquinoline as corrosion inhibitors for mild steel in 1.0 M HCl medium. J Mater Environ Sci 9(1):172–188
28. Grimme S, Antony J, Ehrlich S, Krieg H (2010) A consistent and accurateab initioparametrization of density functional dispersion correction (DFT-D) for the 94 elements H-Pu. J Chem Phys 132: 154104–154119
29. Laabaissi M, Rbaa M, Ourrak M, Zarrok A, El Faydy M, Lakhrissi B, Oudda H (2018) Adsorption Properties and Inhibition of Carbon Steel Corrosion in Hydrochloric Acid Solution by Novel Diazepine Derivatives: Experimental and Theoretical Studies. J Mater Environ Sci 9(6):1796–1808
30. Elfaydy M, Lgaz H, Salghi R, Larouj M, Jodeh S, Rbaa M, Oudda H, Toumiat K, Lakhrissi B (2016) Investigation of Corrosion Inhibition Mechanism of Quinoline Derivative on Mild Steel in 1.0 M HCl Solution: Experimental, Theoretical and Monte Carlo Simulation. J Mater Environ Sci 7(9):3193–3210
31. Saha SK, Hens A, RoyChowdhury A, Lohar AK, Murmu NC, Banerjee P (2014) Molecular dynamics and density functional theory study on corrosion inhibitory action of three substituted pyrazine derivatives on steel surface. Can Chem Trans 2:489–503
32. Saha SK, Ghosh P, Hens A, Murmu NC, Banerjee P (2015) Density functional theory and molecular dynamics simulation study on corrosion inhibition performance of mild steel by mercapto-quinoline Schiff base corrosion inhibitor. Phys E 6:332–341
33. Obot IB, Gasem ZM (2014) Theoretical evaluation of corrosion inhibition performance of some pyrazine derivatives. Corros Sci 83:359–366
34. Yadav DK, Quraishi MA, Maiti B (2012) Inhibition effect of some benzylidenes on mild steel in 1 M HCl: An experimental and theoretical correlation. Corros Sci 55:254–266
35. Ouakki M, Rbaa M, Galai M, Lakhrissi B, Rifi EH, Cherkaoui M (2018) Experimental and quantum chemical investigation of imidazole derivatives as corrosion inhibitors on mild steel in 1.0 M hydrochloric acid. J Bio Tribo Corros 4(3):35
36. Dkhireche N, Galai M, El Kacimi Y, Rbaa M, Ouakki M, Lakhrissi B, Ebn Touhami M (2018) New Quinoline derivatives as sulfuric acid inhibitor's for mild steel. Anal Bioanal Electrochem 10(1): 111–135
37. Eddy NO (2011) Experimental and theoretical studies on some amino acids and their potential activity as inhibitors for the corrosion of mild steel, part 2. J Adv Res 2:35–47
38. Riggs OL Jr (1973) Corrosion inhibition, second ed., C.C. Nathan, Houston, TX
39. Ahamad I, Quraishi MA (2010) Mebendazole: New and efficient corrosion inhibitor for mild steel in acid medium. Corros Sci 52: 651–656
40. Zhang F, Tang Y, Cao Z, Jing W, Wu Z, Chen Y (2012) Performance and theoretical study on corrosion inhibition of 2-(4-pyridyl)-benzimidazole for mild steel in hydrochloric acid. Corros Sci 61:1–9
41. Popova A, Christov M, Vasilev A (2007) Inhibitive properties of quaternary ammonium bromides of N-containing heterocycles on acid mild steel corrosion. Part II: EIS results. Corros Sci 49:3290–3302
42. Popova A, Sokolova E, Raicheva S, Christov M (2003) AC and DC study of the temperature effect on mild steel corrosion in acid media in the presence of benzimidazole derivatives. Corros Sci 45:33–58
43. Krishnegowda PM, Venkatesha VT, Krishnegowda PKM, Shivayogiraju SB (2013) Acalypha torta leaf extract as green corrosion inhibitor for mild steel in hydrochloric acid solution. Ind Eng Chem Res 52:722–728
44. Fares MM, Maayta AK, Al-Qudah MM (2012) Pectin as promising green corrosion inhibitor of aluminum in hydrochloric acid solution. Corros Sci 60:112–117
45. Singh AK, Shukla SK, Quraishi MA, Ebenso EE (2012) Investigation of adsorption characteristics of N, N′-[(methylimino) dimethylidyne] di-2, 4-xylidine as corrosion inhibitor at mild steel/sulphuric acid interface. J Taiwan Inst Chem Eng 43:463–472
46. Saha SK, Dutta A, Ghosh P, Sukul D, Banerje P (2016) Novel Schiff-base molecules as efficient corrosion inhibitors for mild steel surface in 1 M HCl medium: experimental and theoretical approach. Phys Chem Chem Phys 18:17898–17911
47. Zarrouk A, Zarrok H, Ramli Y, Bouachrine M, Hammouti B, Sahibed-dine A, Bentiss F (2016) Inhibitive properties, adsorption and theoretical study of 3,7-dimethyl-1-(prop-2-yn-1-yl)quinoxalin-2(1H)-one as efficient corrosion inhibitor for carbon steel in hydrochloric acid solution. J Mol Liq 222:239–252
48. Obot IB, Obi-Egbedi NO, Eseola AO (2011) Anticorrosion potential of 2-mesityl-1h-imidazo[4,5-f][1,10]phenanthroline on mild steel in sulfuric acid solution: experimental and theoretical study. Ind Eng Chem Res 50:2098–2110

49. Bereket G, Hür E, Öğretir C (2002) Quantum chemical studies on some imidazole derivatives as corrosion inhibitors for iron in acidic medium. J Mol Struct 578(1):79–88
50. Kumar AM, Babu RS, Obot IB, Gasem ZM (2015) Fabrication of nitrogen doped graphene oxide coatings: experimental and theoretical approach for surface protection. RSC Adv 5:19264–19272
51. Obot IB, Ebenso EE, Kabanda MM (2013) Metronidazole as environmentally safe corrosion inhibitor for mild steel in 0.5 M HCl: Experimental and theoretical investigation. J Environ Chem Eng 1: 431–439
52. Obot IB, Umoren SA, Gasem ZM, Suleiman R, El Ali B (2015) Theoretical prediction and electrochemical evaluation of vinylimidazole and allylimidazole as corrosion inhibitors for mild steel in 1 M HCl. J Ind Eng Chem 21:1328–1339